Journal of Materials Chemistry A

RSC Publishing

PAPER

View Article Online
View Journal

Cite this: DOI: 10.1039/c3ta11182b

Triindole-cored star-shaped molecules for organic solar cells†

Zhen Lu,[ab] Cuihong Li,*[a] Tao Fang,[a] Guangwu Li[a] and Zhishan Bo*[a]

Received 24th March 2013
Accepted 22nd April 2013

DOI: 10.1039/c3ta11182b

www.rsc.org/MaterialsA

Two new triindole-cored star-shaped molecules **SM-1** and **SM-2** have been designed and synthesized, and their optical, electrochemical, thermal, transport and photovoltaic properties have been investigated in detail. **SM-1** and **SM-2** exhibited good thermal stability, intensive absorption in a broad region, and relatively high hole mobility. Photovoltaic performances of these two molecules were investigated by fabricating bulk heterojunction solar cell devices with a blend film of **SM-1**:$PC_{71}BM$ or **SM-2**:$PC_{71}BM$ as the active layer. Organic solar cells (OSCs) based on **SM-1**:$PC_{71}BM$ and **SM-2**:$PC_{71}BM$ gave power conversion efficiencies (PCEs) of 2.05% and 2.29%, respectively. A PCE of 2.29% is the best result for all the reported triindole-based photovoltaic materials, indicating that triindole-based small molecules could become promising donor materials for solution-processed OSCs.

Introduction

In recent years, organic and polymer solar cells based on the concept of the bulk heterojunction active layer structure have received increasing scientific attention due to their advantages such as light weight, low cost, flexibility, *etc.*[1] Power conversion efficiency (PCE) of polymer solar cells has reached 9.2%,[2] however some disadvantages of polymer donor materials such as batch to batch variation, difficult purification, broad molecular weight distribution, end-group contamination, *etc.* may retard their future practical applications. Although the PCE of the known organic molecule-based solar cells is still lower than that of polymer-based solar cells, organic molecule-based solar cells are still considered promising for their obvious advantages such as easy purification, no batch to batch variation, defined molecular structure, *etc.*[3] Many new small organic molecule donor materials based on triphenylamine,[4] oligothiophene,[5] hexabenzocoronene,[6] diketopyrrolopyrrole,[7] benzothiadiazole,[8] 1,2,5-thiadiazolo[3,4-*c*]pyridine,[9] and dithienosilole[10] have recently been reported. Very recently the PCE of small organic molecule based solar cells has reached 7%,[10c,11] endowing small organic molecules with a great application potential. However, the development of small organic molecule donor materials still lags behind polymer materials due to their low PCE and poor film forming properties.

Triindole, which resembles truxene, is a planar conjugated aromatic molecule with strong electron-donating ability. Triindole has been used as building block in the construction of functional materials for two-photon absorption,[12] organic light-emitting diodes,[13] and discotic liquid crystals.[14] However, the use of triindole as an electron donating core for the fabrication of planar star-shaped molecules, which could be used as donor materials for organic solar cell (OSC) applications, is rarely reported.[15] Here we report our recent results on the design and synthesis of two novel triindole cored star-shaped molecules, **SM-1** and **SM-2** as shown in Chart 1, for high efficiency organic solar cells (OSCs). For **SM-1**, the triphenylamine (TPA) donor unit is on the periphery of the star-shaped molecular and the benzothiadiazole acceptor unit is located at the center of the arm. For **SM-2**, the acceptor unit is located at the periphery of the star molecule. The photophysical properties of these two molecules were investigated in detail. These two star-shaped small organic molecules exhibited good solubility in common organic solvents such as toluene and 1,2-dichlorobenzene

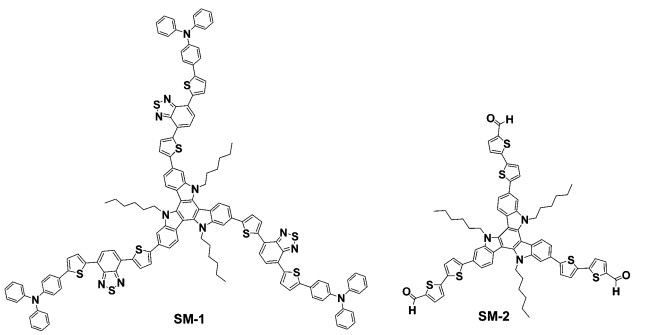

Chart 1 The structures of **SM-1** and **SM-2**.

[a]*Beijing Key Laboratory of Energy Conversion and Storage Materials, College of Chemistry, Beijing Normal University, Beijing 100875, China. E-mail: licuihong@bnu.edu.cn; zsbo@bnu.edu.cn; Fax: +86 10 62206891; Tel: +86 10 62206891*

[b]*College of Chemistry and Chemical Engineering, ShanXi DaTong University, DaTong 037009, China*

† Electronic supplementary information (ESI) available. See DOI: 10.1039/c3ta11182b

(DCB), and bulk heterojunction organic solar cells (BHJ OSCs) were fabricated with **SM-1** or **SM-2** as the donor and $PC_{71}BM$ as the acceptor. Field-effect transistor (OFET) results showed that these two molecules display high hole mobility. PCEs of 2.05 and 2.29% have been achieved for **SM-1**:$PC_{71}BM$ and **SM-2**:$PC_{71}BM$ based solar cells, respectively.

Experimental section

Materials and instruments

^1H and ^{13}C NMR spectra were recorded on a Bruker AV 400 spectrometer. MALDI-TOF was recorded on a Bruker Daltonics Reflex III. Elemental analyses were performed on a Flash EA 1112 analyzer. Fluorescence spectra were recorded on a FluoroMax-4 spectrofluorometer. UV-visible absorption spectra were obtained on a PerkinElmer UV-vis spectrometer model Lambda 750. Thermal gravimetric analysis (TGA) and differential scanning calorimetry (DSC) measurements were performed on TA 2100 and Perkin-Elmer Diamond DSC instruments, respectively, under a nitrogen atmosphere at a heating rate of 20 °C min^{-1} to record TGA and DSC curves. The thickness of the blend films was determined by a Dektak 6M surface profilometer. The electrochemical behavior of the star molecules was investigated using cyclic voltammetry (CHI 630A Electrochemical Analyzer) with a standard three-electrode electrochemical cell in a 0.1 M tetrabutylammonium tetrafluoroborate solution in CH_3CN at room temperature, under an atmosphere of nitrogen with a scanning rate of 0.1 V s^{-1}. A Pt plate working electrode, a Pt wire counter electrode, and an $Ag/AgNO_3$ (0.01 M in CH_3CN) reference electrode were used. The experiments were calibrated with the standard ferrocene/ferrocenium (F_c) redox system and the assumption that the energy level of F_c is 4.8 eV below vacuum. Atomic force microscopy (AFM) measurements were performed under ambient conditions using a Digital Instrument Multimode Nanoscope IIIA operating in the tapping mode. Unless otherwise noted, all chemicals were purchased from Aldrich or Acros and used without further purification. The catalyst precursor $Pd(PPh_3)_4$ was prepared according to the literature and stored in a Schlenk tube under nitrogen atmosphere. Hexane and dichloromethane (DCM) were distilled from CaH_2. Chloroform (CF) was distilled before use. All reactions were performed under an atmosphere of nitrogen and monitored by thin layer chromatography (TLC) on silica gel 60 F254 (Merck, 0.2 mm). Column chromatography was carried out on silica gel (200–300 mesh).

Fabrication and characterization of organic field-effect transistors (OFETs)

Top-contact devices were fabricated based on Si/SiO_2 substrates (the back low resistance Si as gate, SiO_2 (500 nm) with a capacitance of 7.5 nF cm^{-2} as gate insulator). The Si/SiO_2 substrate was sequentially cleaned with water, hot concentrated sulfuric acid–hydrogen peroxide solution (2 : 1 by volume), water, ethanol, and pure acetone, and then treated with trichloro(octadecyl)silane (OTS) by the normal vapor deposition method described elsewhere. Sample films were spin-coated on the OTS modified Si/SiO_2 substrates from CF solutions with a **SM-1** or **SM-2** concentration of 10 mg mL^{-1}. Au electrodes (25 nm) were vacuum deposited on sample films with width/length = 50 (channel width = 2.5 mm, channel length = 50 um). *J–V* characteristics were obtained using an Agilent B2902A Source Meter with a Micromanipulator 6150 probe station in a clean and shielded box at room temperature in air.

Solar cell fabrication and characterization

Small molecular organic solar cells (SMOSCs) were fabricated with the device configuration of ITO/PEDOT:PSS/**SM-1** or **SM-2**:$PC_{71}BM$/LiF/Al. The conductivity of ITO was 20 Ω $\square^{-1}$. PEDOT:PSS is Baytron Al 4083 from H.C. Starck and was filtered with a 0.45 mm poly(vinylidene fluoride) (PVDF) film before use. A thin layer of PEDOT:PSS was spin-coated on top of cleaned ITO substrate at 3000 rpm s^{-1} for 60 s and dried subsequently at 120 °C for 30 min on a hotplate before being transferred into a glove box. The thickness of the PEDOT:PSS layer was about 40 nm. The blend of star molecules and $PC_{71}BM$ was dissolved in DCB and heated at 90 °C overnight to ensure the sufficient dissolution, and then spin-coated onto PEDOT:PSS layer. The top electrode was thermally evaporated, with a 0.5 nm LiF layer, followed by 100 nm of aluminum at a pressure of 10^{-4} Pa through a shadow mask. Five cells were fabricated on one substrate with an effective area of 0.04 cm^2. The measurement of devices was conducted in air without encapsulation. Current–voltage characteristics were recorded using an Agilent B2902A Source Meter under an AM1.5G AAA class solar simulator (model XES-301S, SAN-EI) with an intensity of 100 mW cm^{-2} as the white light source, and the intensity was calibrated with a standard single-crystal Si photovoltaic cell. The temperature while measuring the *J–V* curves was approximately 25 °C.

6-Bromo-*N*-hexylisatin (2). A mixture of 6-bromoisatin (**1**) (22.6 g, 100 mmol), potassium carbonate (K_2CO_3) (41.4 g, 300 mmol), $C_6H_{13}I$ (17.8 mL, 120 mmol), and *N*,*N*-dimethylformamide (DMF) (100 mL) was stirred at 70 °C for 8 h under a nitrogen atmosphere. The mixture was allowed to cool to room temperature, poured into water, and extracted with DCM (3 × 100 mL); the combined organic layers were dried with anhydrous magnesium sulfate ($MgSO_4$) and evaporated to dryness; and the residue was purified on a silica gel column eluted with ethyl acetate (EA) : petroleum ether (PE) (1 : 5) to afford **2** as an orange solid (21.2 g, 72%). ^1H NMR (400 MHz, $CDCl_3$): δ (ppm) 7.39–7.37 (d, $J = 7.96$ Hz, 1H), 7.21–7.18 (d, $J = 8.8$ Hz, 1H), 6.99 (s, 1H), 3.64–3.60 (t, $J = 7.32$ Hz, 2H), 1.65–1.57 (m, 2H), 1.32–1.23 (m, 6H), 0.83–0.80 (t, $J = 6.8$ Hz, 6H). ^{13}C NMR (100 MHz, $CDCl_3$): δ (ppm) 182.3, 157.9, 151.8, 133.5, 126.7, 126.3, 116.3, 113.7, 40.4, 31.3, 27.1, 26.5, 22.4, 13.9.

6-Bromo-*N*-hexyloxindole (3). A mixture of compound **2** (10.1 g, 32 mmol), 1,2-diethoxyethane (20 mL), and hydrazine hydrate (80%) was stirred and refluxed for 12 h under a nitrogen atmosphere. The reaction mixture was allowed to cool to room temperature, the resulted precipitates were collected by filtration to afford **3** as a yellow solid (8.8 g, 93%). ^1H NMR (400 MHz, $CDCl_3$): δ (ppm) 7.17–7.15 (d, 1H), 7.11–7.09 (d, 1H), 6.96 (s, 1H),

3.68–3.64 (t, 2H), 3.46 (s, 2H), 1.68–1.61 (m, 2H), 1.36–1.30 (m, 6H), 0.91–0.87 (t, 6H). ^{13}C NMR (100 MHz, $CDCl_3$): δ (ppm) 174.7, 146.2, 125.6, 124.8, 123.4, 121.3, 111.7, 40.2, 35.4, 31.4, 27.3, 26.6, 22.6, 14.0.

2,7,12-Tribromo-5,10,15-trihexyltriindole (4). A solution of **3** (8.8 g, 29.7 mmol) in $POCl_3$ (100 mL) was degassed and stirred at 100 °C overnight. After the removal of $POCl_3$ under reduced pressure, water was added, and the mixture was neutralized with concentrated NaOH to pH = 7–8. The mixture was extracted with DCM (3 × 100 mL), the combined organic layers were dried over anhydrous $MgSO_4$ and evaporated to dryness, and the residue was purified on a silica gel column using DCM/PE (1 : 10, v/v) as eluent to afford **4** as a colorless solid (2.83 g, 34%). ^{1}H NMR (400 MHz, $CDCl_3$): δ (ppm) 7.84–7.82 (d, J = 8.64 Hz, 3H), 7.55 (s, 3H), 7.31–7.29 (d, 3H), 4.53–4.49 (t, 6H), 1.75 (unsolved, 6H), 1.12 (unsolved, 18H), 0.74–0.70 (t, 9H), ^{13}C NMR (100 MHz, $CDCl_3$): δ (ppm) 141.8, 138.5, 122.7, 122.4, 121.8, 116.5, 113.4, 102.9, 46.9, 31.5, 29.6, 26.3, 22.4, 13.8. Anal. calcd for $C_{42}H_{48}Br_3N_3$: C, 60.44; H, 5.80; N, 5.03. Found: C, 60.31; H, 5.86; N, 5.01%.

5,10,15-Trihexyltriindole-2,7,12-triboronic ester (5). A mixture of compound **4** (1.0 g, 1.2 mmol), pinacolborane (1.82 g, 14.4 mmol), triethylamine (2.42 g, 23.96 mmol), and 1,2-dichloroethane (50 mL) was carefully degassed and cooled with an ice-bath before and after the addition of $PdCl_2(PPh_3)_2$ (84 mg, 0.12 mmol). The reaction mixture was stirred at 70 °C for 48 h. After the removal of the solvent under reduced pressure, the crude product was purified on a silica gel column using EA : PE (1 : 5) as eluent to afford **5** as a colorless solid (450 mg, 39%). ^{1}H NMR (400 MHz, $CDCl_3$): δ (ppm) 8.20–8.18 (d, J = 8.0 Hz, 3H), 8.00 (s, 3H), 7.72–7.70 (d, J = 8.0 Hz, 3H), 7.34–7.32 (6H), 4.90–4.87 (t, J = 6.8 Hz, 6H), 1.91–1.84 (unsolved, 6H), 1.35 (unsolved, 36H), 1.19–1.13 (m, 18H), 0.73–0.69 (t, 9H). ^{13}C NMR (100 MHz, $CDCl_3$): δ (ppm) 140.4, 139.9, 126.1, 125.9, 120.7, 116.9, 103.2, 83.7, 46.9, 31.36, 29.8, 26.2, 24.9, 22.4, 13.9. Anal. calcd for $C_{60}H_{84}B_3N_3O_6$: C, 73.85; H, 8.68; N, 4.31. Found: C, 73.84; H, 8.62; N, 4.42%.

4-(5-(4-(5-Bromothiophen-2-yl)benzo[*c*][1,2,5]thiadiazol-7-yl)-thiophen-2-yl)-*N*,*N*-diphenylbenzenamine (6). A mixture of 4,7-bis(5-bromothiophen-2-yl)benzo[*c*][1,2,5]thiadiazole (1.00 g, 2.18 mmol) and triphenylamine boronic ester (810 mg, 2.18 mmol), K_2CO_3 (6.00 g, 43.6 mmol), Bu_4NBr (140 mg, 0.44 mmol), toluene (200 mL), and water (50 mL) was carefully degassed before and after $Pd(PPh_3)_4$ (126 mg, 0.11 mmol) was rapidly added. The reaction mixture was stirred at 120 °C under a nitrogen atmosphere for 3 days. The organic layer was separated; the aqueous one was extracted with DCM (3 × 100 mL); the combined organic layers were dried over anhydrous $MgSO_4$ and the solvent was removed. The residue was chromatographically purified on a silica gel column eluting with PE/toluene (2 : 1) to afford **6** as a red solid (350 mg, 26%). ^{1}H NMR (400 MHz, $CDCl_3$): δ (ppm) 8.03–8.02 (d, 1H), 7.74–7.69 (m, 3H), 7.50–7.47 (d, 2H), 7.24–7.20 (5H), 7.08–7.07 (m, 5H), 7.03–6.97 (unsolved, 4H), ^{13}C NMR (100 MHz, $CDCl_3$): δ (ppm) 152.4, 152.3, 147.7, 147.4, 145.7, 140.8, 130.6, 129.4, 128.9, 127.9, 126.9, 126.6, 125.2, 124.7, 123.4, 123.3, 114.4. MS (MALDI-TOF): calcd 622.6, found (M^+) 622.4.

5-(Thiophen-2-yl)thiophene-2-carbaldehyde (7). A mixture of 2-thiophene boronic pinacol ester (5.50 g, 26.2 mmol), 5-bromothiophene-2-carbaldehyde (5.00 g, 26.2 mmol), K_2CO_3 (36.1 g, 260 mmol), toluene (200 mL), and water (50 mL) was carefully degassed before and after the addition of $Pd(PPh_3)_4$ (300 mg, 0.26 mmol). The reaction mixture was stirred at 120 °C under a nitrogen atmosphere for 3 days. The organic layer was separated; the aqueous one was extracted with DCM (3 × 100 mL); and the combined organic layers were dried over anhydrous $MgSO_4$ and evaporated to dryness. The residue was chromatographically purified on a silica gel column eluting with DCM to afford **7** as a yellow solid (3.5 g, 69%). ^{1}H NMR (400 MHz, $CDCl_3$): δ (ppm) 9.89 (s, 1H), 7.99 (d, 1H), 7.98–7.69 (d, 1H), 7.59–7.58 (d, 1H), 7.52–7.51(d, 1H), 7.18–7.16 (t, 1H). ^{13}C NMR (100 MHz, $CDCl_3$): δ (ppm) 183.7, 145.6, 141.2, 139.0, 135.2, 128.8, 128.3, 126.9, 125.0.

5-(5-Bromothiophen-2-yl)thiophene-2-carbaldehyde (8). A mixture of compound **7** (1.70 g, 8.75 mmol), tetrahydrofuran (THF) (100 mL), *N*-bromosuccinimide (NBS) (1.53 g, 9.62 mmol), and acetic acid (10 mL) was stirred at 60 °C overnight. The mixture was poured into brine and extracted twice with DCM. The combined organic layers were dried over anhydrous $MgSO_4$ and evaporated to dryness. The crude product was recrystallized from hexane and DCM (1 : 1) to afford **8** as a greenish yellow solid (2.20 g, 97%). ^{1}H NMR (400 MHz, $CDCl_3$): δ (ppm) 9.86 (s, 1H), 7.66–7.65 (d, 1H), 7.18–7.17 (d, 1H), 7.11–7.10 (d, 1H), 7.04–7.03(d, 1H). ^{13}C NMR (100 MHz, $CDCl_3$): δ (ppm) 182.4, 145.8, 142.1, 137.5, 137.1, 131.2, 126.2, 124.4, 114.2.

2,7,12-Tris(4-(4,7-bisthiophenyl)benzo[*c*][1,2,5]thiadiazol-yl)-*N*,*N*-diphenylbenzenamino-yl-5,10,15-trihexyltriindole (SM-1). A mixture of compound **5** (70 mg, 0.071 mmol), compound **8** (200 mg, 0.320 mmol), K_2CO_3 (197 mg, 1.43 mmol), Bu_4NBr (5 mg, 0.014 mmol), toluene (20 mL), and water (3 mL) was carefully degassed before and after the addition of $Pd(PPh_3)_4$ (12.4 mg, 0.011 mmol). The mixture was stirred and refluxed under N_2 for 3 days. Water and CF were added, the organic layer was separated, the aqueous layer was extracted with CF (50 mL × 2), and the combined organic layers were dried over anhydrous $MgSO_4$ and evaporated to dryness. The residues were purified by column chromatography on silica gel eluting with CF/PE (1 : 2, v/v) (5 : 1, v/v) to afford **SM-1** as a purple solid (120 mg, 75%). ^{1}H NMR (500 MHz, $CDCl_3$): δ (ppm) 8.50 (d, 3H), 8.35 (d, 3H), 8.25 (d, 3H), 8.16 (s, 3H), 7.97 (d, 3H), 7.91 (d, 3H), 7.86 (d, 3H), 7.73 (d, 3H), 7.66 (d, 6H), 7.40 (d, 3H), 7.36 (t, 12H), 7.25 (d, 12H), 7.19 (d, 6H), 7.13 (t, 6H), 5.12 (t, 6H), 2.21(p, 6H), 1.53 (p, 6H), 1.40 (p, 6H), 1.34 (p, 2H), 0.96 (t, 9H). ^{13}C NMR (125 MHz, $CDCl_3$): δ (ppm) 152.7, 147.8, 147.6, 146.9, 145.6, 141.9, 139.7, 138.2, 134.9, 134.3, 133.0, 132.8, 132.6, 131.6, 131.1, 130.8, 130.5, 130.4, 130.3, 129.4, 129.3, 129.2, 129.1, 128.5, 128.4, 128.3, 128.2, 128.0, 127.7, 127.4, 126.7, 126.4, 126.2, 125.8, 124.9, 123.7, 123.5, 123.3, 122.2, 118.5, 107.6, 104.1, 47.2, 31.6, 30.0, 26.5, 22.59, 13.90. Anal. calcd for $C_{138}H_{108}N_{12}S_9$: C, 74.56; H, 4.90; N, 7.56. Found: C, 73.93; H, 4.85; N, 7.49%. MS (MALDI-TOF): calcd 2220.6, found (M^+) 2220.4. HRMS: m/z calcd (M^{2+}) 1110.3147, found 1110.3117.

2,7,12-Tris(5-formyl-2,2′-bithiophenyl)-5,10,15-trihexyltriindole (SM-2). A mixture of compound **5** (100 mg, 0.102 mmol), compound **8** (126 mg, 0.461 mmol), K_2CO_3 (281 mg, 2.03 mmol), THF (20 mL), and water (3 mL) was carefully degassed before and after the addition of $Pd(PPh_3)_4$ (12 mg, 0.011 mmol). Then the mixture was heated at 70 °C and stirred under N_2 for 3 days. The mixture was poured into water and extracted with CF. The organic layers were separated, dried over $MgSO_4$, and filtered. After evaporation of solvent, the residues were subjected to column chromatography eluting with CF : PE (5 : 1 by volume) to afford **SM-2** as orange solids (84 mg, 70%). ^{1}H NMR (400 MHz, $CDCl_3$): δ (ppm) 9.83 (s, 3H), 7.76–7.74 (d, 3H), 7.62–7.61 (d, 3H), 7.34 (s, 3H), 7.31–7.29 (d, 3H), 7.26–7.23 (d, 6H), 7.18–7.17 (d 3H), 4.29 (m, 6H), 1.78 (m, 6H), 1.25 (m, 18H), 0.85 (t, 9H). ^{13}C NMR (100 MHz, $CDCl_3$): δ (ppm) 182.3, 147.3, 147.1, 141.2, 140.7, 138.9, 137.5, 134.3, 127.9, 127.2, 123.6, 123.4, 122.6, 121.4, 117.6, 106.7, 102.8, 46.4, 31.3, 29.7, 26.2, 22.5, 14.0. MALDI-TOF MS: calcd 1173.3, found 1173.4 (M^+). Anal. calcd for $C_{69}H_{63}N_3O_3S_6$: C, 70.55; H, 5.41; N, 3.58; found: C, 70.85; H, 5.66; N, 3.50%.

Results and discussion

Synthesis

The syntheses of triindole-cored star-shaped small organic molecules **SM-1** and **SM-2** are shown in Scheme 1. The synthesis of triindole core began from commercially available 6-bromoindoline-2,3-dione (**1**).[12a] Trimerization of **3** in $POCl_3$ at 100 °C afforded 2,7,12-tribromo-5,10,15-trihexyltriindole (**4**) in 32% yield. The key intermediate, 5,10,15-trihexyltriindole-2,7,12-triboronic acid pinacol ester (**5**), was prepared in 39% yield by reaction of **4** and pinacolborane with $PdCl_2(PPh_3)_2$ as the catalyst, triethylamine as the base, and 1,2-dichloroethane as the solvent. The triphenylamine (TPA) terminated arm (**6**) was synthesized by Suzuki–Miyaura cross coupling of 4,7-bis(5-bromothiophen-2-yl)benzo[*c*][1,2,5]thiadiazole and triphenylamine boronic acid pinacol ester in 29% yield. The desired triindole-cored star-shaped small organic molecule **SM-1** was achieved in a yield of 75% by Suzuki–Miyaura cross coupling of the boronic acid pinacol ester functionalized triindole core (**5**) and TPA-terminated bromo functionalized arm (**6**). The synthesis of formyl terminated **SM-2** included three steps. Suzuki–Miyaura cross-coupling of 5-bromothiophene-2-carbaldehyde and 2-thiophene boronic acid pinacol ester with $Pd(PPh_3)_4$ as the catalyst precursor afforded 5-(thiophen-2-yl) thiophene-2-carbaldehyde (**7**) in 69% yield. Bromination of (**7**) with NBS in a solvent mixture of THF and acetic acid furnished 5-(5-bromothiophen-2-yl)thiophene-2-carbaldehyde (**8**) in a yield of 97%. Finally, the attachment of the arm (**8**) to the boronic acid pinacol ester terminated core **5** by Suzuki–Miyaura cross-coupling reaction furnished the desired star-shaped molecule **SM-2** in a yield of 70%.

Optical properties

UV-vis absorption spectra of **SM-1** and **SM-2** in dilute CF solutions and as films are shown in Fig. 1. Samples used for the measurement of film absorption spectra were prepared by spin-coating with CF solutions. The corresponding absorption data are summarized in Table 1. In dilute CF solution, **SM-1** exhibits two distinct absorption bands, the band peaking at 380 nm in the shorter wavelength region originates from the triindole units, and the band in the longer wavelength region peaking at 542 nm is from internal charge transfer (ICT) absorption. The molar absorption coefficient value of the ICT absorption peak at 542 nm is 1.07×10^5 M^{-1} cm^{-1}, which is weaker than that of the short wavelength absorption peak at 380 nm (1.45×10^5 M^{-1} cm^{-1}). On going from solution to film, the absorption spectrum of **SM-1** became broader and the two absorption peaks red-shifted to 393 nm and 572 nm, respectively. For **SM-1**, a red-shift of about 30 nm is probably due to the weak aggregation of star-shaped molecules in the film. The film absorption onset of **SM-1** is at about 680 nm, corresponding to an optical band gap of 1.82 eV. The formyl terminated star-shaped molecule **SM-2** displayed a broad absorption in the visible region with a weak short wavelength absorption peak and an intense long wavelength ICT absorption peak, which are located at 347 nm and 445 nm, respectively. Molar absorption coefficient values of the ICT absorption peak and the short wavelength absorption peak originating from the triindole core are 1.22×10^5 M^{-1} cm^{-1} and 8.96×10^4 M^{-1} cm^{-1}, respectively. Compared with the solution absorption spectrum of **SM-2**, the corresponding film absorption spectrum became much broader and the two absorption peaks red-shifted to 372 nm and 486 nm, respectively. The film absorption onset of **SM-2** is at about 598 nm, corresponding to an optical band gap of 2.07 eV.

Electrochemical properties

Electrochemical properties of **SM-1** and **SM-2** were investigated by cyclic voltammetry (CV). The onset potential of the F_c/F_{c^+} redox couple was found to be 0.09 V relative to the Ag/AgCl reference electrode. Samples used for CV measurements were drop-cast from CF solutions of **SM-1** or **SM-2** on the Pt plate working electrode. The CV curves are shown in Fig. 2 and the data are summarized in Table 1. The onset oxidation potentials of **SM-1** and **SM-2** are 0.41 V and 0.36 V, respectively, in the scanning range of 0 to 1.5 V. The highest occupied molecular orbital (HOMO) energy level was determined by the equation $E_{HOMO} = -e(E_{ox} + 4.71)$ (eV) and the lowest unoccupied molecular orbital (LUMO) energy level was calculated by the equation $E_{LUMO} = E_{HOMO} + E_{g,opt}$. The HOMO and LUMO energy levels of **SM-1** were calculated to be −5.12 and −3.30 eV, respectively. The HOMO and LUMO energy levels of **SM-2** were calculated to be −5.07 and −3.00 eV, respectively. Considering that $PC_{61}BM$ or $PC_{71}BM$ has HOMO and LUMO energy levels of around −6.0 and −4.2 eV, respectively,[16] when **SM-1** and **SM-2** are used as donor materials and $PC_{61}BM$ or $PC_{71}BM$ as acceptor material for the fabrication of organic solar cells, their energy levels will be compatible.

Thermal properties

Thermal properties of **SM-1** and **SM-2** were investigated by thermogravimetric analysis (TGA) and differential scanning

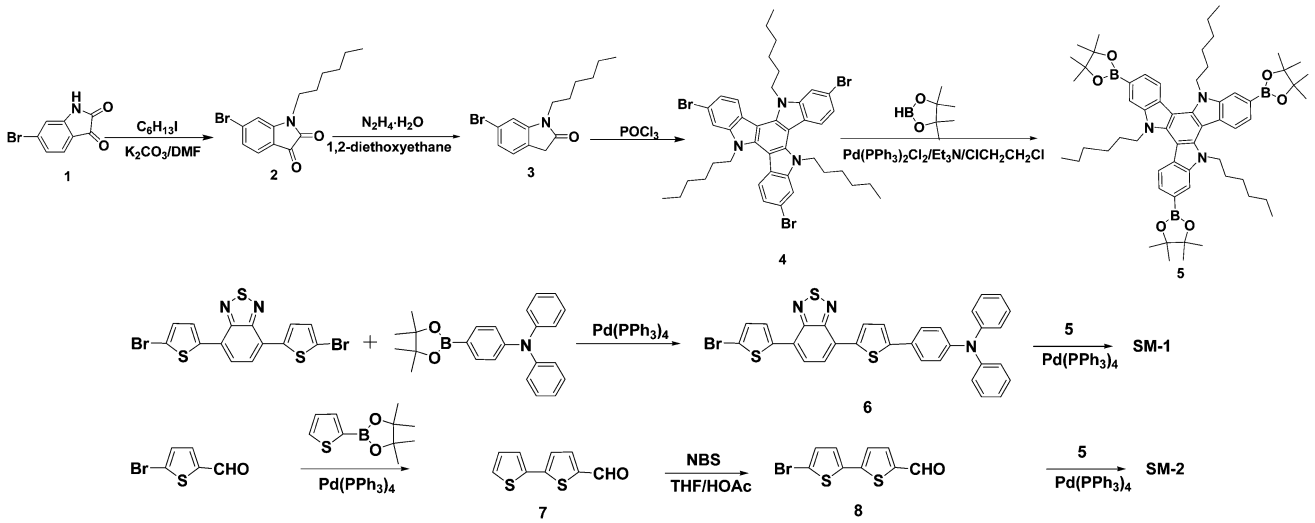

Scheme 1 Synthesis of **SM-1** and **SM-2**.

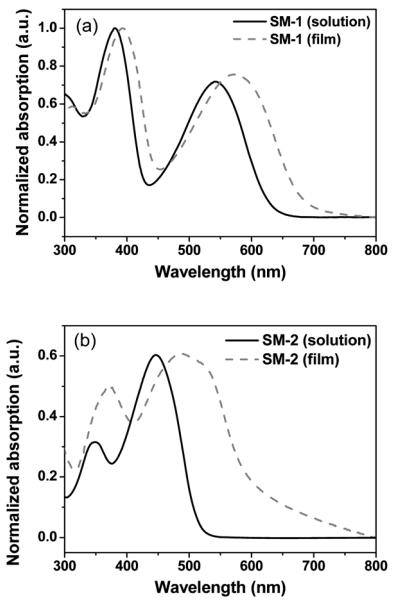

Fig. 1 UV-vis absorption spectra of **SM-1** and **SM-2** in CF solutions and as thin films.

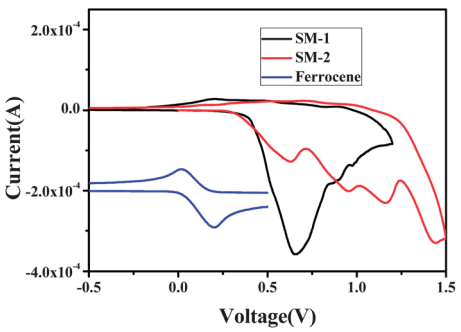

Fig. 2 Cyclic voltammetry (CV) curves of **SM-1** (a) and **SM-2** (b) in films with a scan rate of 100 mV s^{-1} in 0.10 M Bu_4NPF_6 acetonitrile solution.

calorimetry (DSC) under a nitrogen atmosphere at a rate 20 °C min^{-1}. As shown in Fig. 3, **SM-1** and **SM-2** displayed a 5% weight loss at 425 °C and 392 °C, respectively, indicating that they are of good thermal stability. DSC measurements showed that these two star-shaped molecules have no glass transition in the range of 50 °C to 300 °C.

Organic solar cells

BHJ OSCs were fabricated with triindole-cored star-shaped organic molecule **SM-1** or **SM-2** as the electron donor and $PC_{71}BM$ as the electron acceptor. $P_{71}CBM$ instead of $P_{61}CBM$ was chosen as the electron acceptor due to its stronger absorption in the visible region.[17] Photovoltaic properties were examined in BHJ OSCs with a device structure of ITO/PEDOT:PSS/active layer/LiF/Al. The active layer is a blend of **SM-1** or **SM-2** and $PC_{71}BM$, spin-coated from DCB solutions at different weight ratios. The performance of the organic solar cells based on these two star-shaped molecules is very sensitive to the ratio of donor to acceptor. For both **SM-1** and **SM-2**, a donor to acceptor ratio of 1 : 3 by weight and an active layer thickness of about 105 nm have been optimized to give the best

Table 1 Electrochemical, optical, and transport properties of **SM-1** and **SM-2**

	λ_{max} [nm] solution	λ_{max} [nm] film	Film absorption onset [nm]	$E_{g,opt}$ [eV]	E_{ox} [V]	HOMO	LUMO	μ [cm^2 V^{-1} s^{-1}]
SM-1	380, 542	393, 572	680	1.82	0.41	−5.12	−3.30	4.0×10^{-4}
SM-2	346, 447	371, 486	598	2.07	0.36	−5.07	−3.00	3.9×10^{-4}

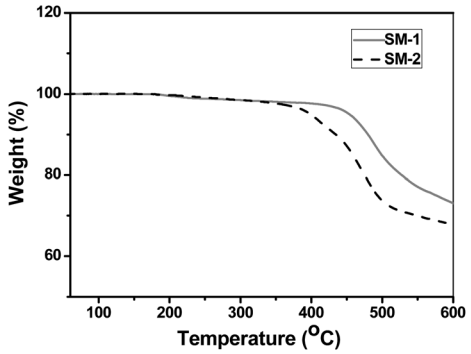

Fig. 3 TGA traces of **SM-1** and **SM-2** measured at a heating rate 20 °C min^{-1} and a N_2 flow of 50 mL min^{-1}.

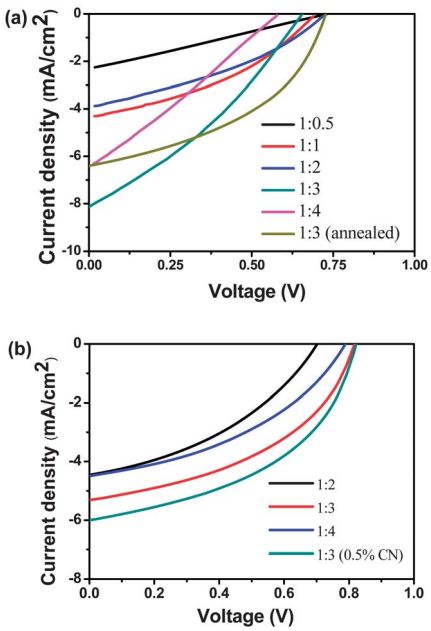

Fig. 4 *J–V* curves of BHJ OSCs with **SM-1**:$PC_{71}BM$ (a) and **SM-2**:$PC_{71}BM$ (b) in different weight ratios as the active layer.

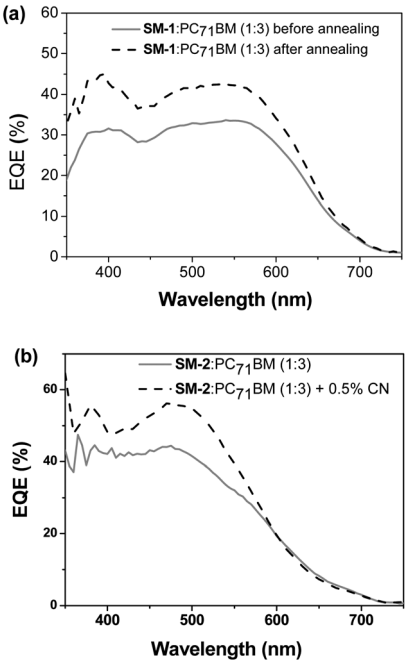

Fig. 5 EQE curves of solar cells based on **SM-1**:$PC_{71}BM$ (1 : 3 by weight) blends from DCB solutions before and after annealing (a) and **SM-2**:$PC_{71}BM$ (1 : 3 by weight) blends from DCB solutions with and without 0.5% CN as the additive (b).

performance. *J–V* curves of the optimized OSC devices under the illumination of AM 1.5G solar spectrum simulator (100 mW cm^{-2}) are shown in Fig. 4, and the results are summarized in Table 2. As shown in Table 2, the optimized devices based on **SM-1**:$PC_{71}BM$ (1 : 3 by weight) gave a PCE of 1.73% with a V_{oc} of 0.65 V, an FF of 0.33, and a J_{sc} of 8.13 mA cm^{-2}. The PCE could be further improved to 2.05% after thermal annealing at 130 °C for 5 min. For **SM-2**, the optimized devices based on **SM-2**:$PC_{71}BM$ (1 : 3, by weight) showed a PCE of 1.95% with a V_{oc} of 0.82 V, an FF of 0.45, and a J_{sc} of 5.31 mA cm^{-2}. The PCE could be improved to 2.29% after the use of 0.5% 1-chloronaphthalene (CN) as an additive.[18] The external quantum efficiency (EQE), which is determined by illumination with monochromatic light, is a significant parameter for evaluating the

Table 2 Photovoltaic properties of **SM-1**:$PC_{71}BM$ and **SM-2**:$PC_{71}BM$ based organic solar cells

Active layer	Weight ratio	V_{oc} (V)	J_{sc} (mA cm^{-2})	FF	PCE %	Thickness (nm)
SM-1/$PC_{71}BM$	1 : 0.5	0.74	2.32	0.25	0.44	106
SM-1/$PC_{71}BM$	1 : 1	0.73	3.95	0.35	1.01	101
SM-1/$PC_{71}BM$	1 : 2	0.70	4.65	0.36	1.17	105
SM-1/$PC_{71}BM$	1 : 3	0.65	8.13	0.33	1.73	104
SM-1/$PC_{71}BM$	1 : 4	0.58	6.47	0.26	1.02	110
SM-1/$PC_{71}BM^a$	1 : 3	0.72	6.41	0.44	2.05	105
SM-2/$PC_{71}BM$	1 : 2	0.70	4.46	0.40	1.23	95
SM-2/$PC_{71}BM$	1 : 3	0.82	5.31	0.45	1.95	103
SM-2/$PC_{71}BM$	1 : 4	0.79	4.49	0.41	1.45	105
SM-2/$PC_{71}BM^b$	1 : 3	0.82	6.00	0.47	2.29	105

[a] The blend film was treated at 130 °C for 5 min in N_2. [b] 0.5% CN as the additive.

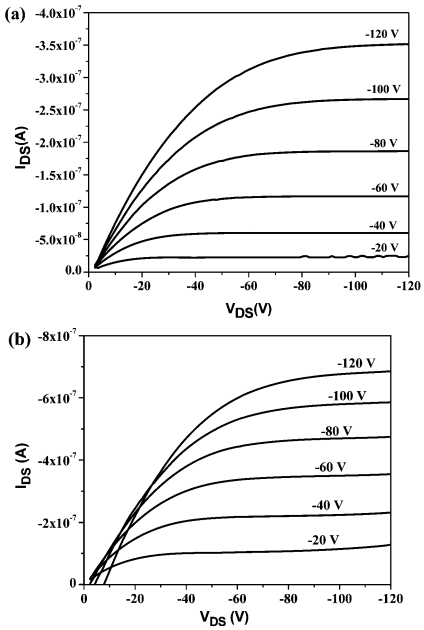

Fig. 6 The output curves of spin-coated films of **SM-1** (a) and **SM-2** (b) on OTS-treated Si/SiO_2 substrates.

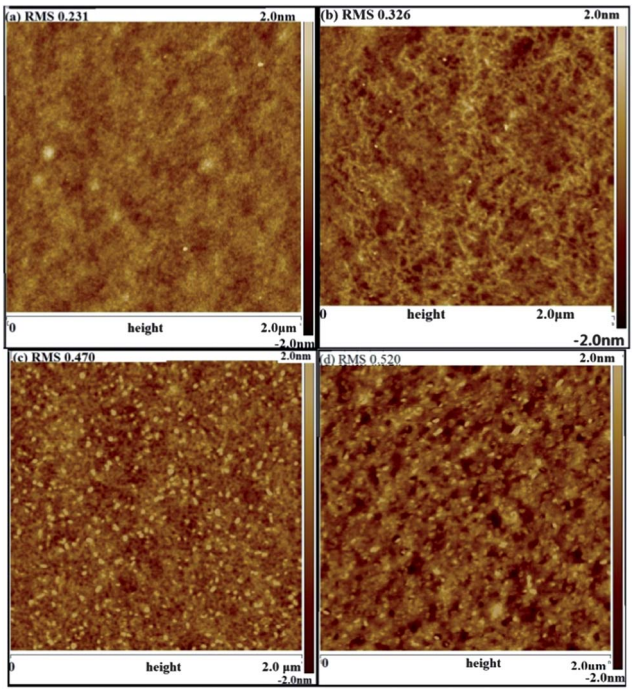

Fig. 7 AFM height images of **SM-1**:P_{71}CBM (1 : 3 by weight) blend before (a) and after (b) annealing at 130 °C for 5 min; AFM height images of **SM-2**:P_{71}CBM (1 : 3 by weight) blend without additive (c) and with 0.5% CN additive (d) (2×2 μm^2).

photovoltaic performance of solar cells. EQE curves of devices based on **SM-1**:$PC_{71}BM$ (1 : 3 by weight) before and after annealing at 130 °C for 5 min and **SM-2**:$PC_{71}BM$ (1 : 3 by weight) with and without 0.5% CN as an additive are shown in Fig. 5. **SM-1**/$PC_{71}BM$ (1 : 3 by weight) based devices exhibited a broader EQE response in the range of 350 to 610 nm with a maximum of 42% at 535 nm. After annealing, the device exhibited a higher EQE response in the whole range of 350 to 610 nm with a maximum of 33% at 535 nm. Devices based on **SM-2**/$PC_{71}BM$ (1 : 3 by weight) showed a photo-to-current response in the range of 380 to 600 nm with a maximum EQE of 44% at 475 nm. When using 0.5% CN as the additive for the fabrication of devices, the maximum EQE could be further increased to 55%. The current intensity (J_{sc}) values calculated from the integration of EQEs agree well with the J_{sc} values obtained from the $J-V$ measurements.

Transport properties

The photovoltaic performance is closely related to the transport properties of the active layer, and high power efficiency organic solar cells require the organic donor and $PC_{61}BM$ or $PC_{71}BM$ blends to have a balanced electron and hole mobility to promote the continuous generation of electrons without recombination or saturation of charges. $PC_{61}BM$ has an electron mobility of 2×10^{-3} cm^2 V^{-1} s^{-1}; donor materials usually have lower hole mobility, and therefore intensive research has been carried out to pursue high hole mobility donor materials. The transport properties of these two star-shaped molecules were investigated by fabricating OFETs. The OFET devices of **SM-1** and **SM-2** exhibited typical p-channel field-effect transistor behavior. The hole mobility (μ) was estimated in the saturated regime from the derivative plots of the square root of source-drain current (I_{SD}) *versus* gate voltage (V_G) through the equation $I_{SD} = (W/2L)C_i\mu(V_G - V_T)^2$ where W is the channel width, L is the channel length, C_i is the capacitance per unit area of the gate dielectric layer (SiO_2, 500 nm, $C_i = 7.5$ nF cm^{-2}), and V_T is the threshold voltage. The output curves of the spin-coated film of **SM-1** and **SM-2** on OTS-treated Si/SiO_2 substrates are shown in Fig. 6. The hole mobilities and the on/off ratio are listed in Table 1. Without further device optimization, the hole mobility of **SM-1** film spin coated from CF solution is 4.0×10^{-4} cm^2 V^{-1} s^{-1} with an on/off ratio of 2.0×10^2. The hole mobility of **SM-2** film spin coated from CF solution is 3.9×10^{-4} cm^2 V^{-1} s^{-1} with an on/off ratio of 1.0×10^2. These results indicate that **SM-1** and **SM-2** are promising donor materials for organic solar cell applications.

Morphology

The morphology of blend films, which has a significant influence on the charge separation and transportation, was investigated by AFM in tapping-mode.[19] Samples used for AFM investigations were prepared by spin-coating from DCB solutions. AFM images of blend films of **SM-1** and $PC_{71}BM$ (1 : 3 by weight) before and after annealing at 130 °C for 5 min are shown in Fig. 7a and b, respectively.

Before annealing, the blend films showed a rather smooth surface with a root-mean-square (rms) roughness value of 0.231; whereas after annealing, the blend films became apparently phase separated and a fibrous structure could be observed with the rms roughness value increasing to 0.326, indicating that the formation of fibrous structures and appropriate phase separation are favorable for charge separation and transport. For

SM-2, investigations have shown that the PCE of the devices can be improved by the use of 0.5% CN as the additive. Therefore, samples used for AFM investigations were prepared by spin-coating from DCB solutions of **SM-2** and $PC_{71}BM$ in a weight ratio of 1 : 3 without and with 0.5% CN as the additive. As shown in Fig. 7c, the blend film of **SM-2**:$PC_{71}BM$ (1 : 3 by weight) spin-coated from DCB solution showed a smooth surface with smaller phase separation and the rms roughness value is 0.47. After the use of 0.5% CN as the additive, the morphology of the active layer became rougher with obviously larger phase separation and the rms roughness value is creased to 0.52 (Fig. 7d). This result indicates that the use of a small amount of additive can markedly change the morphology of blend films and thus improve their photovoltaic performance.

Conclusions

In summary, two new triindole-cored star-shaped molecules **SM-1** and **SM-2** have been designed and synthesized, and their optical, electrochemical, thermal, transport and photovoltaic properties have been investigated in detail. These two star-shaped molecules exhibited good thermal stability, intense absorption in a broad region, and relatively high hole mobility. The photovoltaic performances of these two molecules were investigated by fabricating bulk heterojunction solar cell devices with a blend film of **SM-1**:$PC_{71}BM$ or **SM-2**:$PC_{71}BM$ as the active layer. OSCs based on **SM-1**:$PC_{71}BM$ and **SM-2**:$PC_{71}BM$ gave PCEs of 2.05% and 2.29%, respectively. A PCE of 2.29% is the best result for all the reported triindole-based photovoltaic materials, indicating that triindole-based small molecular could become promising donor materials for solution-processed OSCs. However, the PCE of triindole based solar cells is still far below the highest PCE of 7% reported for small molecule organic solar cells.[10c,11] The low PCE for these two triindole-based small organic is probably due to their relatively wide optical band gap and high HOMO energy level, which will result in smaller J_{sc} and lower V_{oc}, respectively. We expect that we can further increase the PCE of organic solar cells by designing and synthesizing new triindole cored star molecules with stronger peripheral acceptor units such as dicyanovinyl group. With these aims, we feel that triindole cored star-shaped molecules are worth further exploration as donor materials for high efficiency small molecular solar cells.

Acknowledgements

We thank the financial support by the 973 Program (2011CB935703 and 2009CB623603), the NSF of China (91233205, 21161160443 and 51003006), and the Fundamental Research Funds for the Central Universities.

Notes and references

1 (*a*) C. J. Brabec, S. Gowrisanker, J. J. M. Halls, D. Laird, S. J. Jia and S. P. Williams, *Adv. Mater.*, 2010, **22**, 3839–3856; (*b*) J. W. Chen and Y. Cao, *Acc. Chem. Res.*, 2009, **42**, 1709–1718; (*c*) G. Dennler, M. C. Scharber and C. J. Brabec, *Adv. Mater.*, 2009, **21**, 1323–1338; (*d*) C. Du, C. H. Li, W. W. Li, X. Chen, Z. S. Bo, C. Veit, Z. F. Ma, U. Wuerfel, H. F. Zhu, W. P. Hu and F. L. Zhang, *Macromolecules*, 2011, **44**, 7617–7624; (*e*) J. H. Hou, H. Y. Chen, S. Q. Zhang, G. Li and Y. Yang, *J. Am. Chem. Soc.*, 2008, **130**, 16144–16145; (*f*) L. J. Huo, S. Q. Zhang, X. Guo, F. Xu, Y. F. Li and J. H. Hou, *Angew. Chem., Int. Ed.*, 2011, **50**, 9697–9702; (*g*) H. J. Jiang, X. Y. Deng and W. Huang, *Prog. Chem.*, 2008, **20**, 1361–1374; (*h*) J. Y. Kim, K. Lee, N. E. Coates, D. Moses, T. Q. Nguyen, M. Dante and A. J. Heeger, *Science*, 2007, **317**, 222–225; (*i*) F. C. Krebs, *Sol. Energy Mater. Sol. Cells*, 2009, **93**, 394–412; (*j*) S. H. Park, A. Roy, S. Beaupre, S. Cho, N. Coates, J. S. Moon, D. Moses, M. Leclerc, K. Lee and A. J. Heeger, *Nat. Photonics*, 2009, **3**, 297–302; (*k*) S. C. Price, A. C. Stuart, L. Q. Yang, H. X. Zhou and W. You, *J. Am. Chem. Soc.*, 2011, **133**, 4625–4631; (*l*) R. P. Qin, W. W. Li, C. H. Li, C. Du, C. Veit, H. F. Schleiermacher, M. Andersson, Z. S. Bo, Z. P. Liu, O. Inganas, U. Wuerfel and F. L. Zhang, *J. Am. Chem. Soc.*, 2009, **131**, 14612–14613; (*m*) J. S. Song, C. Du, C. H. Li and Z. S. Bo, *J. Polym. Sci., Part A: Polym. Chem.*, 2011, **49**, 4267–4274; (*n*) E. G. Wang, Z. F. Ma, Z. Zhang, K. Vandewal, P. Henriksson, O. Inganas, F. L. Zhang and M. R. Andersson, *J. Am. Chem. Soc.*, 2011, **133**, 14244–14247.

2 Z. C. He, C. M. Zhong, S. J. Su, M. Xu, H. B. Wu and Y. Cao, *Nat. Photonics*, 2012, **6**, 591–595.

3 (*a*) Y. Z. Lin, Y. F. Li and X. W. Zhan, *Chem. Soc. Rev.*, 2012, **41**, 4245–4272; (*b*) J. Roncali, *Acc. Chem. Res.*, 2009, **42**, 1719–1730; (*c*) B. Walker, C. Kim and T. Q. Nguyen, *Chem. Mater.*, 2011, **23**, 470–482.

4 (*a*) C. He, Q. G. He, Y. P. Yi, G. L. Wu, F. L. Bai, Z. G. Shuai and Y. F. Li, *J. Mater. Chem.*, 2008, **18**, 4085–4090; (*b*) S. Roquet, A. Cravino, P. Leriche, O. Aleveque, P. Frere and J. Roncali, *J. Am. Chem. Soc.*, 2006, **128**, 3459–3466; (*c*) H. X. Shang, H. J. Fan, Y. Liu, W. P. Hu, Y. F. Li and X. W. Zhan, *Adv. Mater.*, 2011, **23**, 1554–1557.

5 (*a*) R. Fitzner, C. Elschner, M. Weil, C. Uhrich, C. Korner, M. Riede, K. Leo, M. Pfeiffer, E. Reinold, E. Mena-Osteritz and P. Bauerle, *Adv. Mater.*, 2012, **24**, 675–680; (*b*) S. Haid, A. Mishra, M. Weil, C. Uhrich, M. Pfeiffer and P. Bauerle, *Adv. Funct. Mater.*, 2012, **22**, 4322–4333; (*c*) Z. Li, G. R. He, X. J. Wan, Y. S. Liu, J. Y. Zhou, G. K. Long, Y. Zuo, M. T. Zhang and Y. S. Chen, *Adv. Energy Mater.*, 2012, **2**, 74–77.

6 (*a*) J. Li, M. Kastler, W. Pisula, J. W. F. Robertson, D. Wasserfallen, A. C. Grimsdale, J. Wu and K. Mullen, *Adv. Funct. Mater.*, 2007, **17**, 2528–2533; (*b*) W. W. H. Wong, C. Q. Ma, W. Pisula, C. Yan, X. L. Feng, D. J. Jones, K. Mullen, R. A. J. Janssen, P. Bauerle and A. B. Holmes, *Chem. Mater.*, 2010, **22**, 457–466; (*c*) W. W. H. Wong, T. B. Singh, D. Vak, W. Pisula, C. Yan, X. L. Feng, E. L. Williams, K. L. Chan, Q. H. Mao, D. J. Jones, C. Q. Ma, K. Mullen, P. Bauerle and A. B. Holmes, *Adv. Funct. Mater.*, 2010, **20**, 927–938.

7 (*a*) J. H. Liu, B. Walker, A. Tamayo, Y. Zhang and T. Q. Nguyen, *Adv. Funct. Mater.*, 2013, **23**, 47–56; (*b*) K. A. Mazzio, M. J. Yuan, K. Okamoto and C. K. Luscombe,

ACS Appl. Mater. Interfaces, 2011, **3**, 271–278; (*c*) B. Walker, A. B. Tomayo, X. D. Dang, P. Zalar, J. H. Seo, A. Garcia, M. Tantiwiwat and T. Q. Nguyen, *Adv. Funct. Mater.*, 2009, **19**, 3063–3069.

8 (*a*) W. W. Li, C. Du, F. H. Li, Y. Zhou, M. Fahlman, Z. S. Bo and F. L. Zhang, *Chem. Mater.*, 2009, **21**, 5327–5334; (*b*) Z. L. Wu, B. H. Fan, F. Xue, C. Adachi and J. Y. Ouyang, *Sol. Energy Mater. Sol. Cells*, 2010, **94**, 2230–2237; (*c*) M. C. Yuan, Y. J. Chou, C. M. Chen, C. L. Hsu and K. H. Wei, *Polymer*, 2011, **52**, 2792–2798.

9 (*a*) Y. Sun, S. C. Chien, H. L. Yip, Y. Zhang, K. S. Chen, D. F. Zeigler, F. C. Chen, B. P. Lin and A. K. Y. Jen, *J. Mater. Chem.*, 2011, **21**, 13247–13255; (*b*) C. J. Takacs, Y. M. Sun, G. C. Welch, L. A. Perez, X. F. Liu, W. Wen, G. C. Bazan and A. J. Heeger, *J. Am. Chem. Soc.*, 2012, **134**, 16597–16606; (*c*) G. C. Welch, L. A. Perez, C. V. Hoven, Y. Zhang, X. D. Dang, A. Sharenko, M. F. Toney, E. J. Kramer, T. Q. Nguyen and G. C. Bazan, *J. Mater. Chem.*, 2011, **21**, 12700–12709; (*d*) X. Yong and J. P. Zhang, *J. Mater. Chem.*, 2011, **21**, 11159–11166.

10 (*a*) J. Ohshita, *Macromol. Chem. Phys.*, 2009, **210**, 1360–1370; (*b*) Y. M. Sun, G. C. Welch, W. L. Leong, C. J. Takacs, G. C. Bazan and A. J. Heeger, *Nat. Mater.*, 2012, **11**, 44–48; (*c*) T. S. van der Poll, J. A. Love, T. Q. Nguyen and G. C. Bazan, *Adv. Mater.*, 2012, **24**, 3646–3649.

11 J. Y. Zhou, X. J. Wan, Y. S. Liu, Y. Zuo, Z. Li, G. R. He, G. K. Long, W. Ni, C. X. Li, X. C. Su and Y. S. Chen, *J. Am. Chem. Soc.*, 2012, **134**, 16345–16351.

12 (*a*) L. Ji, Q. Fang, M. S. Yuan, Z. Q. Liu, Y. X. Shen and H. F. Chen, *Org. Lett.*, 2010, **12**, 5192–5195; (*b*) J. J. Shao, Z. P. Guan, Y. L. Yan, C. J. Jiao, Q. H. Xu and C. Y. Chi, *J. Org. Chem.*, 2011, **76**, 780–790.

13 (*a*) W. Y. Lai, Q. Y. He, R. Zhu, Q. Q. Chen and W. Huang, *Adv. Funct. Mater.*, 2008, **18**, 265–276; (*b*) W. Y. Lai, R. Zhu, Q. L. Fan, L. T. Hou, Y. Cao and W. Huang, *Macromolecules*, 2006, **39**, 3707–3709; (*c*) T. H. Zhu, G. K. He, J. Chang, D. D. Zhao, X. L. Zhu and H. J. Zhu, *Dyes Pigm.*, 2012, **95**, 679–688.

14 (*a*) E. M. Garcia-Frutos, A. Omenat, J. Barbera, J. L. Serrano and B. Gomez-Lor, *J. Mater. Chem.*, 2011, **21**, 6831–6836; (*b*) B. Gomez-Lor, B. Alonso, A. Omenat and J. L. Serrano, *Chem. Commun.*, 2006, 5012–5014; (*c*) M. Talarico, R. Termine, E. M. Garcia-Frutos, A. Omenat, J. L. Serrano, B. Gomez-Lor and A. Golemme, *Chem. Mater.*, 2008, **20**, 6589–6591; (*d*) S. Van Cleuvenbergen, I. Asselberghs, E. M. Garcia-Frutos, B. Gomez-Lor, K. Clays and J. Perez-Moreno, *J. Phys. Chem. C*, 2012, **116**, 12312–12321.

15 (*a*) S. W. Shelton, T. L. Chen, D. E. Barclay and B. W. Ma, *ACS Appl. Mater. Interfaces*, 2012, **4**, 2534–2540; (*b*) T. Bura, N. Leclerc, S. Fall, P. Leveque, T. Heiser and R. Ziessel, *Org. Lett.*, 2011, **13**, 6030–6033.

16 T. Erb, U. Zhokhavets, G. Gobsch, S. Raleva, B. Stuhn, P. Schilinsky, C. Waldauf and C. J. Brabec, *Adv. Funct. Mater.*, 2005, **15**, 1193–1196.

17 T. Yamanari, T. Taima, J. Sakai and K. Saito, *Jpn. J. Appl. Phys.*, 2008, **47**, 1230–1233.

18 (*a*) J. S. Moon, C. J. Takacs, S. Cho, R. C. Coffin, H. Kim, G. C. Bazan and A. J. Heeger, *Nano Lett.*, 2010, **10**, 4005–4008; (*b*) X. Guo, C. H. Cui, M. J. Zhang, L. J. Huo, Y. Huang, J. H. Hou and Y. Li, *Energy Environ. Sci.*, 2012, **5**, 7943–7949; (*c*) J. Jo, A. Pron, P. Berrouard, W. L. Leong, J. D. Yuen, J. S. Moon, M. Leclerc and A. J. Heeger, *Adv. Energy Mater.*, 2012, **2**, 1397–1403; (*d*) J. S. Wu, C. T. Lin, C. L. Wang, Y. J. Cheng and C. S. Hsu, *Chem. Mater.*, 2012, **24**, 2391–2399.

19 (*a*) L. Ye, S. Q. Zhang, W. Ma, B. H. Fan, X. Guo, Y. Huang, H. Ade and J. H. Hou, *Adv. Mater.*, 2012, **24**, 6335–6341; (*b*) G. Fang, J. Liu, Y. Y. Fu, B. Meng, B. H. Zhang, Z. Y. Xie and L. X. Wang, *Org. Electron.*, 2012, **13**, 2733–2740; (*c*) J. E. Carle, B. Andreasen, T. Tromholt, M. V. Madsen, K. Norrman, M. Jorgensen and F. C. Krebs, *J. Mater. Chem.*, 2012, **22**, 24417–24423; (*d*) A. Kumar, Z. R. Hong, S. Sista and Y. Yang, *Adv. Energy Mater.*, 2011, **1**, 124–131; (*e*) H. W. Tang, G. H. Lu and X. N. Yang, *IEEE J. Sel. Top. Quantum Electron.*, 2010, **16**, 1725–1731; (*f*) M. Shin, H. Kim, J. Park, S. Nam, K. Heo, M. Ree, C. S. Ha and Y. Kim, *Adv. Funct. Mater.*, 2010, **20**, 748–754; (*g*) H. Hoppe, M. Niggemann, C. Winder, J. Kraut, R. Hiesgen, A. Hinsch, D. Meissner and N. S. Sariciftci, *Adv. Funct. Mater.*, 2004, **14**, 1005–1011.